DOI: 10.26599/FSHW.2026.9251192

Contents lists available at SciOpen

Food Science and Human Wellness

journal homepage: https://www.sciopen.com/journal/2097-0765

China Food Publishing Co.

Polystyrene Microplastics Exacerbate Polycystic Ovary Syndrome via Gut Microbiota-Dependent Depletion of Vitamin B6 in Mice

Yue Pan[a, b†], Xiaoqin Zeng[b†], Shulei Chen[c†], Ziwei Zhou[c], Yanzhen Ye[a], Zhihua Zuo[d], Shanshui Zeng[e], Xiaodong Fu[f,*], Yan Long[g,*], Zuman Dou[h,*], Min Jiang[g,*]

[a] *Department of Obstetrics, School of Medicine, the Sixth Affiliated Hospital of South China University of Technology (Nanhai District People's Hospital of Foshan), Foshan, 528200, China*

[b] *Department of Gynecology, Guangzhou Women and Children's Medical Center, Guangzhou Medical University, Guangzhou, Guangdong 510627, China*

[c] *Microbiome Medicine Center, Department of Laboratory Medicine, Zhujiang Hospital, Southern Medical University, Guangzhou, Guangdong 510260, China*

[d] *The Second Clinical Medical College of North Sichuan Medical College; Department of Clinical Laboratory, Beijing Anzhen Nanchong Hospital，Capital Medical University & Nanchong Central Hospital, Nanchong 637000, China*

[e] *Department of Science Innovation, Shenzhen Hospital, Southern Medical University, Shenzhen, Guangdong 518101, China*

[f] *Key Laboratory of Cardiovascular Diseases, Guangzhou Municipal and Guangdong Provincial Key Laboratory of Protein Modification and Degradation, School of Basic Medical Sciences, Guangzhou Medical University, Guangzhou, Guangdong 511436, China*

[g] *Department of Laboratory Medicine, Guangzhou Women and Children's Medical Center, Guangzhou Medical University, Guangzhou, Guangdong 510627, China*

[h] *College of Ocean Food and Biological Engineering, Jimei University, Xiamen, Fujian 361021, China*

ABSTRACT: Microplastics (MPs) have become a widespread environmental contaminant, but their impact on female reproductive health remains poorly understood. Here, we demonstrate that polystyrene microplastics (PS-MPs) exacerbate polycystic ovary syndrome (PCOS) by altering the gut microbiota, leading to vitamin B6 depletion and activation of inflammatory pathways in the ovary. In a DHEA-induced PCOS mouse model, oral exposure to PS-MPs disturbed the intestinal microbial community, marked by reduced *Firmicutes* and elevated *Bacteroidetes*, and caused a pronounced decline in both intestinal and systemic vitamin B6 levels. The abundance of *Flavonifractor plautii*, a key vitamin B6–producing bacterium, declined markedly, correlating with increased ovarian TNF-α and IL-6 expression and activation of the MAPK and NF-κB pathways. These molecular changes were accompanied by oxidative stress, disrupted estrous cyclicity, and abnormal hormone profiles. Notably, oral vitamin B6 supplementation reversed many of these alterations, restoring microbial balance, antioxidant capacity, and ovarian function. Together, these findings identify a gut–vitamin B6–ovary axis that mediates the reproductive toxicity of microplastics. This study reveals a previously unrecognized nutritional mechanism linking environmental exposure to endocrine disruption and suggests that maintaining micronutrient homeostasis may help mitigate microplastic-associated reproductive risks.

Keywords: emerging food contaminants, microplastics, Vitamin B6, gut microbiota, polycystic ovary syndrome

† Yue Pan, Yan Long, Xiaoqin Zeng and Shulei Chen contribute equally to this work.
***Corresponding author**
jiangmin2011@126.com (M. Jiang). dzman320@163.com (Z. Dou).
longyangmc@163.com (Y. Long).fuxiaod@gzhmu.edu.cn (X.D. Fu).

Received 20 November 2025
Received in revised from 4 January 2026
Accepted 11 February 2026

1. Introduction

The pervasive environmental contamination by microplastics (MPs)—synthetic polymer particles smaller than 5 mm—has emerged as a major ecological and public health concern[1]. MPs are now ubiquitous in terrestrial and aquatic systems and have been detected across diverse dietary sources, including drinking water, seafood, table salt, and even fresh produce[2,3]. As persistent anthropogenic pollutants, MPs exhibit remarkable chemical stability, bioaccumulation potential, and biological reactivity, allowing them to interact with living systems in complex ways[4]. Increasing evidence indicates that chronic exposure to MPs can induce oxidative stress, inflammation, and immune dysregulation, thereby contributing to metabolic and endocrine disturbances[5–7]. As evidence accumulates, MPs are increasingly recognized not only as inert particles, but as a new class of endocrine-disrupting contaminants capable of altering systemic physiology. However, while epidemiological data directly linking MP exposure to specific female reproductive disorders like PCOS remains sparse, growing toxicological evidence from animal models raises significant concerns. Furthermore, the potential mechanistic pathways, particularly those involving the gut microbiome and its metabolic output, are largely unexplored.

Female reproductive health appears particularly vulnerable to environmental stressors. Pollutants such as bisphenols, phthalates, dioxins, and heavy metals have been implicated in menstrual irregularities, ovulatory dysfunction, and infertility[8–10]. Polycystic ovary syndrome (PCOS) is the most common endocrine disorder in women of reproductive age, affecting approximately 6–10% globally[11]. It is characterized by hyperandrogenism, oligo- or anovulation, and polycystic ovarian morphology, often accompanied by insulin resistance, obesity, and low-grade inflammation[12]. Although genetic predisposition contributes to PCOS, the rapid rise in global prevalence suggests an essential role for environmental and metabolic factors[13,14]. Recent animal studies show that polystyrene MPs (PS-MPs) impair reproductive hormone synthesis, ovarian function, and insulin sensitivity, suggesting a potential link between microplastic exposure and PCOS-like phenotypes[15]. Exposure to PS-MPs, during critical periods of development, such as in utero or during puberty, may have long-term effects on reproductive health[15,16]. Although the direct link between PS-MPs and PCOS is not yet established, the potential for PS-MPs to interfere with hormone signaling pathways raises concerns about their role in the development and progression of PCOS. Further research is needed to better understand the effects of PS-MPs on reproductive health and to develop strategies to mitigate their potential impact.

The gastrointestinal tract is the primary entry site for ingested MPs and a central hub of host–environment interaction[17,18]. The gut microbiota plays an essential role in nutrient metabolism, immune regulation, and hormonal balance[19]. Dysbiosis of gut microbial communities has been implicated in obesity, diabetes, and reproductive disorders, including PCOS[13,20–22]. Recent studies show that microplastics can disturb gut microbial composition, reduce microbial diversity, and promote local inflammation and barrier dysfunction[23,24]. Importantly, dysbiosis is increasingly recognized as a critical driver of PCOS pathophysiology, influencing androgen synthesis, insulin resistance, and ovarian inflammation[13,25]. These

findings raise an important but unresolved question: could MP-induced gut dysbiosis mechanistically contribute to reproductive dysfunction?

Microbial-derived vitamins serve as critical biochemical mediators between the gut and peripheral organs. Among them, vitamin B6 (pyridoxine and its active form pyridoxal 5'-phosphate) participates in amino acid and glucose metabolism, neurotransmitter synthesis, and antioxidant defense[26]. Deficiency in vitamin B6 has been linked to increased oxidative stress, elevated inflammatory cytokines, and altered steroid hormone synthesis[27]—all pathological hallmarks of PCOS. Given that many intestinal bacteria, particularly within the phylum *Firmicutes*, are capable of synthesizing vitamin B6, perturbations in gut microbial composition may directly affect vitamin B6 availability and downstream reproductive function[28]. Nonetheless, whether environmental microplastics can disrupt this microbial–vitamin–hormone axis remains unknown.

In this study, we investigated the impact of oral PS-MPs exposure on PCOS progression using a dehydroepiandrosterone (DHEA)-induced mouse model. We further examined how PS-MPs-induced gut dysbiosis affects vitamin B6 metabolism and explored whether vitamin B6 supplementation could reverse these effects. Through integrated microbiome, metabolome, and molecular analyses, we identify a gut–vitamin B6–ovary axis linking microplastic exposure to reproductive and metabolic dysfunction.

2. Materials and methods

2.1 Microplastic preparation and characterization

Polystyrene particles within the 1–10 μm range were generated by initially cooling commercial polystyrene beads with dry ice to −78 °C. Once solidified, the material was subjected to continuous homogenization for approximately 4–5 hours to mechanically reduce particle size. The resulting mixture was subsequently fractionated using sequential mesh filtration, first with a 50-μm sieve followed by a 10-μm sieve, to obtain the desired particle fraction. To remove residual contaminants, the collected particles were rinsed repeatedly-four to five times-with ethanol. The cleaned particles were then placed in an oven and dehydrated at 50 °C for 48 hours. A particle size analyzer was used to quantify both particle diameter and zeta potential, while their surface structure was visualized through scanning electron microscopy (SEM). Ultrapure water served as the dispersing medium during characterization.

2.2 Treatment of animals

Three-week-old female C57BL/6 mice were purchased from Bestest Biotechnology Co., Ltd. (Zhuhai, China) and randomly distributed into experimental groups, with 3–5 animals housed per cage. All mice were kept under specific pathogen-free conditions with controlled temperature (22°C), a 12-h light/dark cycle, and unrestricted access to food and water. All procedures were performed in accordance with the guidelines approved by the Animal Care and Use Committee of Guangzhou Medical University (Approval ID: 2018-593).

Human exposure to microplastics has been reported to average between 0.2–10.2 mg/kg/day[29,30]. Using the body surface area (BSA) conversion factor of 12 to extrapolate doses for mice, the estimated equivalent

exposure range was calculated as 2.4–122 mg/kg/day[31]. Based on these estimations, 2 mg/kg/day and 100 mg/kg/day were chosen as the low- and high-dose PS-MPs exposure levels for the mouse experiments.

2.2.1 PS-MPs administration

To assess how PS-MPs influence PCOS-like phenotypes, mice received PS-MPs through drinking water at the predetermined doses over a 20-day period. PCOS-like conditions were induced by daily subcutaneous injections of dehydroepiandrosterone (DHEA, 60 mg/kg; B1375, APExBIO, Houston, USA) dissolved in 0.1 mL sesame oil (S25527, Shanghai Yuanye Biotechnology Co., Ltd., China). A target sample size of n = 10 animals per group was predefined based on preliminary data and standard practice in rodent PCOS models to ensure adequate statistical power while adhering to ethical guidelines. Final group sizes of n = 8 or 9 resulted from predefined exclusions due to unsuccessful DHEA model induction or technical issues during sample collection, all applied prior to data analysis. Control animals received sesame oil only (no DHEA; n = 8), while a baseline PCOS cohort received ultrapure water and DHEA injections without PS-MP exposure (n = 9). To assess the effect of PS-MPs alone, an additional group received the high dose of PS-MPs (2 mg/kg/day or 100 mg/kg/day) in drinking water along with sesame oil injections (no DHEA; n = 8). Experimental PS-MP groups consisted of mice exposed to either 2 mg/kg/day (n = 8) or 100 mg/kg/day (n = 9) PS-MPs combined with DHEA injections.

2.2.2 Fecal microbiota transplantation (FMT)

To investigate the role of PS-MPs in gut microbiota associated with PCOS, fecal microbiota transplantation (FMT) was performed as previously described[32]. Female mice (n = 8 per group) were fasted for 6 h and orally administered 200 μl of an antibiotic cocktail containing 1 g/L ampicillin, 0.5 g/L neomycin, 0.5 g/L vancomycin, and 1 g/L metronidazole for five consecutive days. Beginning the day after antibiotic treatment, mice received 100 μl of gut microbiota suspension by oral gavage every three days for one month, continuing until death or sacrifice. The microbiota suspension was prepared by vortexing 2-5 fresh fecal pellets (80-100 mg) collected from donor mice of the Control, PCOS, or PCOS+HMP groups in 600 μl of reduced PBS (0.5 g/L cysteine, 0.2 g/L sodium sulfide). The mixture was then centrifuged at 2,500 r.p.m. for 1 min, and the supernatant was collected for transplantation. Control recipient mice received the same antibiotic treatment followed by gavage with reduced PBS instead of microbiota suspension.

2.2.3 Vitamin B6 supplementation

To determine whether vitamin B6 alleviates PS-MPs-induced PCOS manifestations, mice in the treatment group were supplied with vitamin B6 (35 mg/mL; Sigma-Aldrich, USA) in their drinking water for 20 days. This supplementation dose was selected based on the following rationale: (1) It corresponds to a daily intake of approximately 350 mg/kg/day (assuming a mouse drinks ~5 mL of water per day and weighs ~25 g), which is within the range used in previous rodent studies to effectively correct vitamin B6 deficiency and exert anti-inflammatory or metabolic benefits[33]; (2) Our preliminary dose-finding experiment indicated that this dose effectively restored serum and ovarian vitamin B6 levels in PS-MPs-exposed mice without observed adverse

effects (data not shown). (3) The aim was to provide a sufficient therapeutic challenge to test the hypothesis that B6 depletion is a key mediator, rather than to mimic a precise human supplementation regimen. Fresh solutions were prepared every 48 hours to ensure stable intake. Control mice consumed the same water without supplementation (n = 10 per group). Environmental conditions and food availability were identical across all groups.

Before euthanasia by cervical dislocation, all mice underwent glucose tolerance (GTT) and insulin tolerance (ITT) tests. Blood samples collected during estrus were used to quantify sex hormone and insulin levels. Following sacrifice, one ovary, colon, and subcutaneous adipose inguinal adipose tissue were fixed in 4% paraformaldehyde, while the remaining ovary, adipose tissue, intestinal segments, and fecal samples were snap-frozen in liquid nitrogen and stored at −80 °C. Fixed tissues were also preserved at −80 °C for further analysis.

2.3 GTT and ITT assay

For the GTT, mice were fasted for 12 h, while a 4-h fasting period preceded the ITT. Blood glucose was measured from tail vein samples using the Accu-Chek Performa glucose meter (Roche Diagnostics). After baseline glucose levels were taken, mice received intraperitoneal injections of insulin (1 IU/kg) for the ITT or D-glucose (2 g/kg) for the GTT. Glucose concentrations were recorded at 15-, 30-, 60-, 90-, and 120-min following injection.

2.4 Vaginal smear test

To assess the impact of DHEA and PS-MPs on estrous cyclicity during the modeling period, we initiated vaginal cytology on day 10 of treatment. Beginning on day 10 of treatment and continuing through day 19, vaginal samples were obtained each morning at 9:00 a.m., ensuring coverage of no fewer than two estrous cycles. Although C57BL/6 females typically attain full, regular estrous cyclicity around 6–7 weeks of age, the subcutaneous administration of the androgen precursor DHEA from 3 weeks of age is intended to disrupt normal pubertal development and estrous cycle establishment. Our monitoring, starting when mice were approximately 5 weeks old, was designed to capture these early disruptions and to ensure we observed at least two full cycle periods before the endpoint of the experiment. After Shorr staining, the slides were analyzed under a microscope to classify the reproductive stage according to the dominant cell population. Preestrus was recognized by the presence of nucleated epithelial cells, whereas estrus was characterized by abundant cornified epithelial cells. Mixed epithelial cells together with leukocytes signified the mid-estrus phase, while late-estrus was defined by increasing leukocyte prevalence accompanied by residual nucleated epithelial cells. All assessments were conducted by investigators blinded to grouping.

2.5 ELISA assay

At the experimental endpoint (day 20), and during the estrus phase as determined by vaginal cytology, mice were anesthetized by intraperitoneal injection of pentobarbital sodium (100 mg/kg, 10% solution in sterile saline; Sigma-Aldrich). After verifying full anesthesia, blood was obtained from the retro-orbital sinus

through enucleation. Samples (approximately 0.8 mL) were centrifuged at 4000 rpm for 20 min at 4 °C, and the separated serum (around 300 μL) was stored at −80 °C for later analysis. Concentrations of testosterone (MM-0569M2), estradiol (MM-0566M2), luteinizing hormone (MM-44039M2) from MEIMIAN Biotech, and insulin (PI602; Beyotime) in serum were determined using ELISA kits, following the manufacturers' protocols. Levels of oxidative stress–related indicators in serum and hippocampal tissues were assessed using colorimetric kits (Nanjing Jiancheng Bioengineering Institute, Nanjing, China), including malondialdehyde (MDA; A003-1-2), glutathione peroxidase (GSH-Px; A005-1-2), superoxide dismutase (SOD; A001-3-2), and total antioxidant capacity (T-AOC; A015-2-1). All experimental steps were performed according to the manufacturers' instructions.

2.6 H&E staining

Ovarian and adipose tissue morphology was evaluated using hematoxylin and eosin (H&E) staining, as previously described[34]. Ovaries and adipose tissues were dissected, rinsed with phosphate-buffered saline (PBS), and fixed in 4% paraformaldehyde. After dehydration through graded ethanol, the tissues were cleared in xylene and embedded in paraffin. Serial 5-μm sections were cut using a microtome, with ovarian sections collected at 50-100 μm intervals to ensure representative sampling. The sections were deparaffinized, rehydrated, and stained with H&E buffer following standard procedures. Stained slides were scanned for whole-slide imaging. Three random fields from each adipose tissue slide were selected for histological scoring. Ovarian morphology was assessed across multiple sections, and follicles at different developmental stages were counted for quantitative analysis.

2.7 Full-length 16s rRNA sequencing

Bacterial community profiling based on the full-length 16S rRNA gene was carried out following methods reported previously[35]. The near-complete 16S rRNA fragment was amplified with primer pair 27F (5′-AGRGTTYGATYMTGGCTCAG-3′) and 1492R (5′-RGYTACCTTGTTACGACTT-3′). PCR reactions were performed in a 10-μL mixture beginning with a 5-minute denaturation at 95 °C, followed by 25 amplification cycles consisting of 95 °C for 30 s, 50 °C for 30 s, and 72 °C for 1 min. The resulting PCR products were sequenced on the PacBio Sequel system (Beijing Personal Biotechnology Co., Ltd.). Raw sequencing data were processed using QIIME2 (v2023.2.0). Amplicon sequence variants (ASVs) were generated by applying the "qiime dada2 denoise-ccs" workflow, and non-bacterial reads—including chloroplast, mitochondrial, and other eukaryotic sequences—and chimeras were removed with "qiime taxa filter-table." Taxonomic assignments were produced using the SILVA v138 reference database through the "qiime feature-classifier" module. To standardize sequencing depth across samples, rarefaction was performed at 4,530 reads per sample using the "qiime diversity core-metrics-phylogenetic" pipeline, from which alpha- and beta-diversity indices were subsequently derived.

2.8 Fecal metabolome assay

A 10 mg sample of feces was accurately weighed and transferred to a sample vial. To extract metabolites,

0.5 mL of 75% aqueous methanol was added, and the mixture was sonicated for 20 minutes. After sonication, the sample was centrifuged at 15,800 g for 20 minutes at 4°C to separate the precipitate. The supernatant was then dried using nitrogen gas. The dried residue was reconstituted with 100 μL of 75% aqueous methanol and subjected to a second centrifugation at 15,800 g for 20 minutes at 4°C. The resulting supernatant was carefully transferred to a new vial. For metabolomic analysis, the samples were processed using an Agilent 1290 Infinity UHPLC system coupled with an AB SCIEX Triple TOF 6600 mass spectrometer. The separation was achieved on a HILIC column maintained at 25°C, with a flow rate of 0.5 mL/min. Gradient elution was performed using mobile phases A (water with 25 mM ammonium acetate and 25 mM ammonia) and B (acetonitrile) as follows: 0-0.5 min, 95% B; 0.5-7 min, B decreased from 95% to 65%; 7-8 min, B decreased from 65% to 40%; 8-9 min, 40% B; 9-9.1 min, B increased from 40% to 95%; 9.1-12 min, 95% B. The autosampler maintained the samples at 4°C throughout the analysis. Mass spectrometry was performed in both positive and negative ESI modes, utilizing optimized source parameters. Full MS scans were collected from 60 to 1000 Da, while MS/MS data were acquired in IDA mode, covering the range of 25 to 1000 Da. To ensure optimal system performance, quality control samples were regularly analyzed. Raw mass spectrometry data were converted to mzXML format using ProteoWizard and processed with XCMS for peak alignment, retention time correction, and peak area extraction. The processed data were subsequently used for metabolite identification and quantification.

2.9 In vitro fermentation

To assess the effects of PS-MPs on vitamin B6 metabolism, an in vitro fermentation model was established. Fresh fecal samples were collected from healthy female participants in the morning using sterile containers. The fermentation medium was prepared as previously described and sterilized by autoclaving at 121 °C for 15 min[36]. Fecal samples were suspended in anaerobic sterile saline, and solid debris was removed by filtration. The resulting suspension was maintained under anaerobic conditions to preserve microbial activity. Sterile fermenters were filled with 50–100 mL of culture medium, and PS-MPs were added at a final concentration of 1mg/L and 10 mg/L for the experimental groups. Subsequently, 20% (v/v) of fecal suspension was inoculated into each fermenter. The fermenters were sealed with airtight rings or placed in anaerobic containers and incubated at 37 °C for 24 h. At designated time points (0, 4, 8, 12, and 16 h), 1 mL of fermentation medium was collected, centrifuged at 10,000 r.p.m. for 10 min, and the supernatant was transferred for metabolite analysis. Vitamin B6 concentrations were determined using high-performance liquid chromatography (HPLC).

2.10 Vitamin B6 quantitative

Vitamin B6 concentrations in serum, ovary, and fecal samples were determined by HPLC. Whole blood was centrifuged at 3,000 r.p.m. for 10 min at 4 °C, and the resulting serum was deproteinized with 0.3 M perchloric acid. After incubation on ice for 10 min, samples were centrifuged at 12,000 r.p.m. for 10 min, and the supernatants were neutralized with 2 M K_2CO_3 and filtered through 0.22 μm membranes. Ovarian tissue (20–50 mg) and fecal samples (50–100 mg) were homogenized in ice-cold 0.3 M perchloric acid, incubated

on ice for 10 min, and centrifuged at 12,000 r.p.m. for 10 min. The supernatants were neutralized, filtered (0.22 μm), and subjected to HPLC analysis. Chromatographic separation was achieved on a C18 reverse-phase column using a phosphate buffer–methanol gradient, and detection was performed at 295 nm. Quantification was based on calibration curves generated with vitamin B6 standards. Concentrations were expressed as pmol/mL for serum and pmol/mg for ovarian and fecal samples.

2.11 Transcriptome sequencing

Total RNA was extracted from the ovaries of mice using Trizol reagent (Invitrogen, Carlsbad, CA, USA) according to standard protocols[37]. RNA integrity was evaluated using the Agilent 2100 Bioanalyzer (Agilent Technologies, Palo Alto, CA, USA) and confirmed by RNase-free agarose gel electrophoresis. To isolate mRNA, ribosomal RNA (rRNA) was removed with the Ribo-Zero™ Magnetic Kit (Epicentre, Madison, WI, USA). The resulting enriched mRNA was fragmented into smaller segments using a fragmentation buffer and subsequently reverse transcribed into complementary DNA (cDNA) with the NEBNext Ultra RNA Library Prep Kit for Illumina (NEB#7530, New England Biolabs, Ipswich, MA, USA). The cDNA was then subjected to end-repair, the addition of an adenine (A) base, and ligation to Illumina-specific sequencing adapters. The ligation products were purified with AMPure XP Beads (1.0X). After PCR amplification, the cDNA library was sequenced on the Illumina Novaseq6000 platform at Gene Denovo Biotechnology Co. (Guangzhou, China). Bioinformatic analysis was carried out on the Omicsmart platform (http://www.omicsmart.com), a real-time, interactive tool for data processing and analysis.

2.12 Real-time quantitative PCR (qPCR) analysis

RNA was isolated from cells using Trizol reagent (Invitrogen, Waltham, MA), following the manufacturer's protocol. qPCR was carried out on an ABI 7500 platform, utilizing SYBR Green PCR Master Mix (Vazyme, Nanjing, China) for amplification. Reactions were prepared in a 20 μL final volume, adhering to the specified guidelines. The thermal cycling conditions included an initial denaturation at 95°C for 2 minutes, followed by 40 cycles of denaturation at 95°C for 10 seconds, and annealing/extension at 60°C for 30 seconds. The primer sequences used are listed in Supplementary Table 1.

2.13 Isolation of primary ovarian granulosa cells

Eight-week-old female C57BL/6 mice were purchased from Bestest Biotechnology Co., Ltd. (Zhuhai, China). All experimental procedures were approved by the Animal Care and Use Committee of Guangdong Laboratory Animal Center. To stimulate follicular development, mice were injected subcutaneously with 10 IU of pregnant mare serum gonadotropin (PMSG). After 48 hours, the mice were euthanized by CO2 inhalation, and ovaries were collected. Granulosa cells were isolated by puncturing the follicles under a dissecting microscope and filtered through a 100 μm nylon mesh. The cells were collected by centrifugation at 1000 rpm and resuspended in DMEM/F12 medium. Cultures of granulosa cells were maintained at 37°C with 5% CO2. Cell identity was confirmed by fluorescent immunostaining for follicle-stimulating hormone receptor (FSHR) (CL594-22665, Proteintech), and only cultures showing more than 90% positivity were used

in the experiments. To assess the impact of pyridoxine (vitamin B6) on MAPK and NF-κB signaling in granulosa cells, pathway activation was triggered with 100 nM phorbol 12-myristate 13-acetate (PMA) for 1 hour. After PMA treatment, cells were incubated with or without 35 mg/mL pyridoxine for 24 hours to evaluate the effects on pathway activation. Western blotting was used to analyze the expression of phosphorylated and total forms of ERK1/2, JNK, p38, IKKα/β, IκBα, and p65, to assess the activation of MAPK and NF-κB signaling pathways.

2.14 Western blot assay

Western blot analysis was carried out according to previously established protocols[38,39]. Protein levels of both total and phosphorylated forms of ERK1/2, JNK, p38 MAPK, IKKα/β, IκBα, and NF-κB p65 were measured in ovarian tissue and granulosa cells from mice. The primary antibodies used for detection included: anti-ERK1/2 (11257-1-AP, Proteintech), anti-phospho-ERK1/2 (28733-1-AP, Proteintech), anti-JNK (66210-1-Ig, Proteintech), anti-phospho-JNK (80024-1-RR, Proteintech), anti-p38 (14064-1-AP, Proteintech), anti-phospho-p38 MAPK (28796-1-AP, Proteintech), anti-IKKα/β (11930, Cell Signaling Technology [CST]), anti-phospho-IKKα/IKKβ (Ser177) (2697, CST), anti-IκBα (4814, CST), anti-phospho-IκBα (2859, CST), anti-p65 (8242, CST), and anti-phospho-NF-κB p65 (3033, CST). As a loading control, β-actin (20536-1-AP, Proteintech) was used. Detection and analysis were conducted using HRP-conjugated secondary antibodies and the Image Lab software.

2.15 Statistics

Data analysis was performed using GraphPad Prism v9.0 and IBM SPSS v23.0 software. To compare differences among three or more groups, one-way ANOVA followed by Tukey's post hoc test was applied. For two-group comparisons, an independent samples t-test was used. Non-parametric tests, including the Mann-Whitney U test for two groups and the Kruskal-Wallis test with Dunn's post hoc analysis for three or more groups, were also performed. Data are expressed as mean ± SD. Correlations were evaluated using Spearman's rank correlation test. A p-value of less than 0.05 was considered statistically significant. One-way ANOVA with Tukey’s or Dunnett’s T3 post hoc tests was applied depending on whether the assumption of homogeneity of variances was satisfied.

3. Results

3.1 Characterization of polystyrene microplastics

PS-MPs were prepared following established protocols[40] and characterized by scanning electron microscopy (SEM) and dynamic light scattering (DLS). SEM analysis revealed that PS-MPs were uniformly spherical with slight surface roughness under high magnification (Fig. S1A). DLS measurements indicated an average diameter of 4.8 ± 0.65 μm (Fig. S1B), while zeta potential analysis showed a near-neutral surface charge (~0 mV) in aqueous suspension (Fig. S1C). These parameters-particle size, morphology, and surface charge—are critical for evaluating the biological effects of PS-MPs in the context of PCOS pathogenesis.

3.2 Oral microplastic exposure exacerbates PCOS characteristics in a DHEA-induced mouse model

Oral gavage of PS-MPs was initially evaluated in age-matched healthy mice. PS-MPs exposure did not induce PCOS-like reproductive phenotypes and resulted only in mild metabolic alterations (Fig. S2). Building on this observation, we established a DHEA-induced PCOS mouse model using 3-week-old female mice and administered low (2 mg/kg/day) or high (100 mg/kg/day) doses of PS-MPs (Fig. 1A) to determine whether microplastic exposure influences disease progression. Treatment with DHEA alone resulted in a slight, non-significant increase in body weight compared to control mice. In contrast, PS-MPs exposure induced a marked, dose-dependent increase in weight, with the high-dose PS-MPs group (PCOS+HMP) showing an average gain of 2.49 ± 1.17 g relative to controls ($P < 0.01$), and (1.46 ± 1.67)g more than the untreated PCOS group (Fig. 1B).

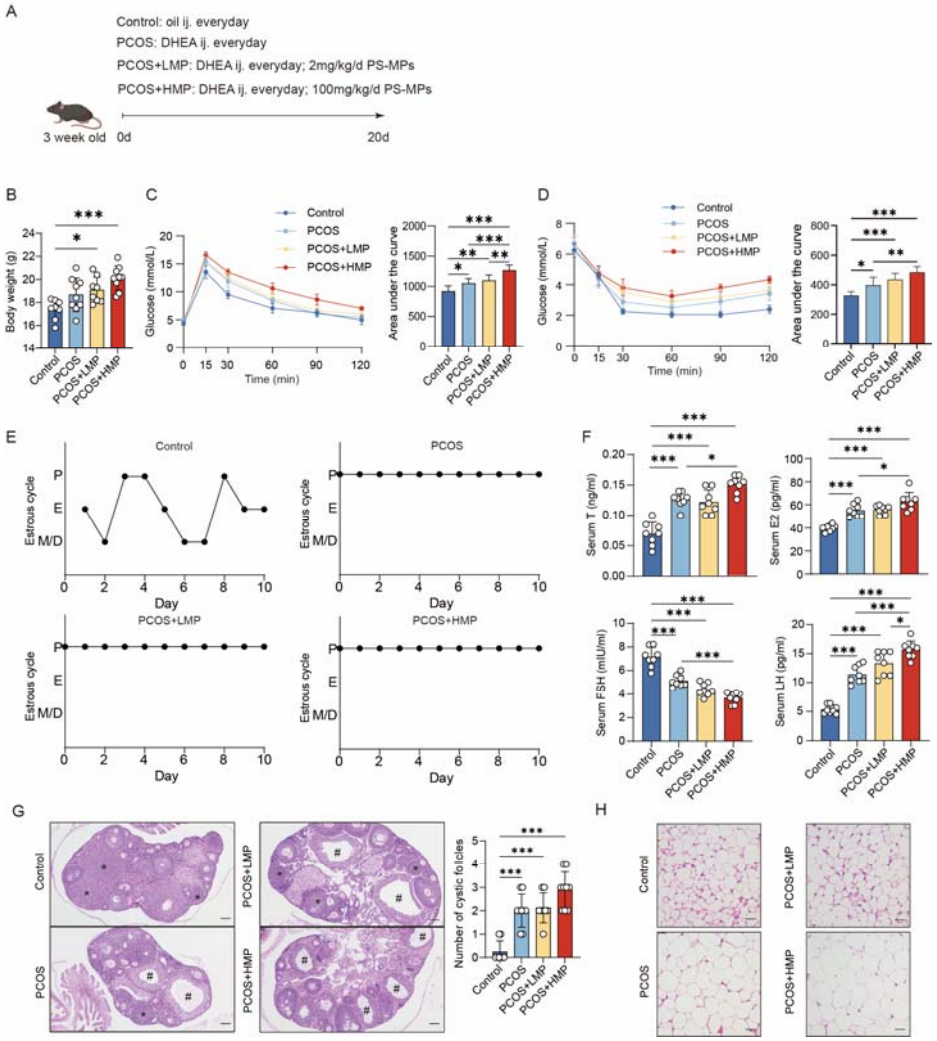

Fig. 1 Exposure to PS-MPs exacerbates disease progression in PCOS mice.

(A) Schematic of experimental design. Three-week-old female mice were subcutaneously injected with DHEA (60 mg/kg/day) and simultaneously exposed to PS-MPs (2 mg/kg/day or 100 mg/kg/day) via drinking water for 20 consecutive days. (B) Body weight, (C) oral glucose tolerance test (OGTT), (D) insulin tolerance test (ITT), and (E) Estrous cycle stages were determined by daily vaginal smears collected from days 10–20. (F) serum levels of testosterone (T), estrogen (E2), luteinizing hormone (LH), and follicle-stimulating hormone (FSH) were measured from blood samples collected at euthanasia on day 20 of the experiment (during the estrus phase) to assess metabolic and endocrine changes. (G) Representative H&E–stained ovarian sections showing follicular morphology (hash symbol, cystic follicles; asterisks, corpora lutea). Scale bar, 200 μm. Quantitative analysis of corpora lutea is shown in Fig. S4A. (H) Representative H&E staining of subcutaneous inguinal adipose tissue showing fat accumulation; scale bar, 200 μm. P, proestrus; E, estrus; M/D, metestrus/diestrus. Data are presented as mean±standard deviation (SD). Results were analyzed by one-way ANOVA followed by Tukey's post hoc test (B, C, D and F) or by Dunnett's T3 multiple comparisons test (G). *$P < 0.05$, **$P < 0.01$, ***$P < 0.001$.

Metabolic evaluations indicated that PS-MPs exposure impaired glucose regulation. Oral glucose tolerance tests (OGTT) demonstrated significant glucose intolerance in a dose-dependent manner (Fig. 1C; $P < 0.01$ for PCOS+HMP vs. Control). Insulin tolerance tests (ITT) also revealed a decrease in insulin sensitivity, particularly pronounced in the PCOS+HMP group (Fig. 1D; $P < 0.001$ vs. Control). These results suggest that PS-MPs exacerbate insulin resistance in this DHEA-induced PCOS model.

DHEA treatment notably disrupted the estrous cycle, with a persistent arrest in the proestrus phase. However, additional exposure to PS-MPs did not induce further changes in the cycle pattern (Fig. 1E). Hormonal measurements revealed elevated levels of testosterone, estrogen, and luteinizing hormone (LH), alongside reduced follicle-stimulating hormone (FSH) in DHEA-treated mice. PS-MPs exposure, particularly at the high dose, aggravated these endocrine disturbances (Fig. 1F). Histological examination of ovaries from PS-MPs-treated mice showed numerous cystic follicles (Fig. 1G) and a significant, dose-dependent reduction in the number of corpora lutea, particularly in the PCOS+HMP group (Fig. S3A; $P < 0.01$ vs. Control and PCOS groups), indicating impaired follicular development and ovulation. Additionally, PS-MPs exposure was associated with increased adiposity in the mice, as evidenced by histology of subcutaneous inguinal adipose tissue (Fig. 1H), which aligns with the observed metabolic dysfunction and insulin resistance.

3.3 PS-MPs exposure promotes ovarian inflammation and oxidative stress

To elucidate the molecular mechanisms underlying PS-MPs–induced ovarian dysfunction, transcriptomic profiling was performed on ovarian tissues from PCOS and PCOS+HMP mice. Compared with the PCOS group, PS-MPs exposure led to a marked upregulation of genes associated with the MAPK and NF-κB signaling pathways (Fig. 2A), implicating these inflammatory cascades in the ovarian response to microplastic exposure. Western blot analysis confirmed these findings, showing a dose-dependent increase in the phosphorylation of ERK, JNK, p38, and NF-κB p65 in PS-MPs–treated ovaries (Fig. 2B).

Consistent with these signaling changes, oxidative stress parameters indicated redox imbalance, characterized by increased malondialdehyde (MDA) levels and decreased total antioxidant capacity (T-AOC), superoxide dismutase (SOD), glutathione (GSH), and glutathione peroxidase (GSH-Px) activities (Fig. 2C, all $P < 0.01$, PCOS+HMP vs. Control). In parallel, inflammatory cytokine analysis revealed markedly elevated *Ifng*, *Cxcl8*, and *Tnfa* transcript levels in the PS-MPs–treated group compared with PCOS controls (Fig. 2D; all $P < 0.01$).

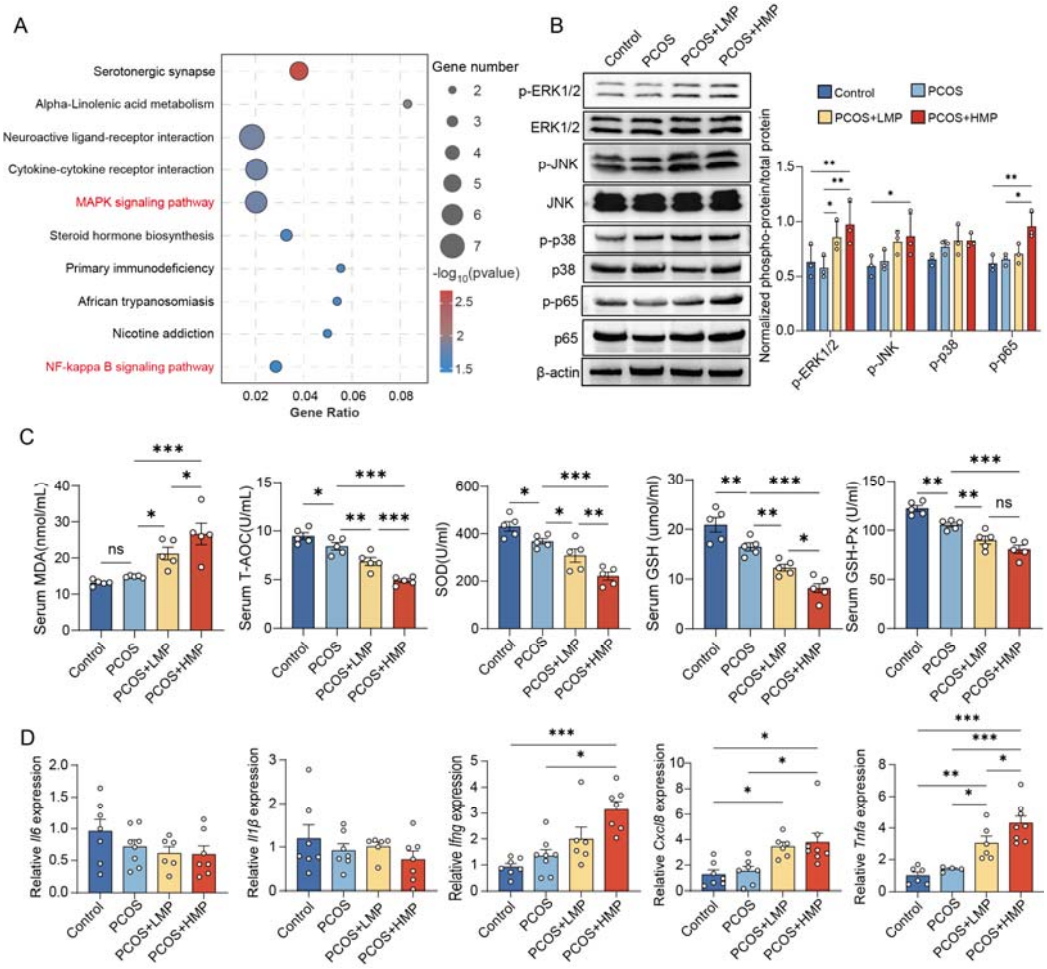

Fig. 2 PS-MPs exposure promotes ovarian inflammation and oxidative stress in PCOS mice. (A) KEGG pathway enrichment analysis of differentially expressed genes in ovarian tissues from PCOS and PCOS+HMP mice. (B) Western blot analysis and quantification of phosphorylated ERK1/2, JNK, p38, and NF-κB p65 in ovarian tissues. β-actin served as the loading control. (C) Oxidative stress markers in serum, including malondialdehyde (MDA), total antioxidant capacity (T-AOC), superoxide dismutase (SOD), glutathione (GSH), and glutathione peroxidase (GSH-Px), showing increased oxidative stress and reduced antioxidant activity after PS-MPs exposure. (D) Relative mRNA expression of inflammatory cytokines (*Il6*, *Il1β*, *Cxcl8*,*Ifng* and *Tnfa*) in ovarian tissue determined by qPCR. Data are presented as mean±standard deviation (SD). Results were analyzed by one-way ANOVA followed by Tukey's post hoc test (C) or by Dunnett's T3 multiple comparisons test (B and D). ns, not significant; *$P < 0.05$, **$P < 0.01$, ***$P < 0.001$.

3.4 PS-MPs exposure disrupts gut microbial composition in PCOS mice

The gastrointestinal tract, a primary site of microplastic exposure, is highly sensitive to microbial disturbances[17,41]. To evaluate whether gut dysbiosis mediates the effects of PS-MPs, histological analysis confirmed that high-dose PS-MPs exposure did not cause overt pathological damage to the colon, liver, or kidneys, and short-term exposure did not increase circulating PS-MPs levels (Fig. S4 and S5).

Gut microbiome analysis revealed that the intake of PS-MPs led to a dose-dependent decrease in α-diversity, with significant reductions observed compared to both the control and PCOS groups. In contrast, no significant differences in α-diversity were detected between the untreated PCOS and control mice (Fig. 3A). Principal coordinate analysis (PCoA) using Bray–Curtis distances further highlighted distinct β-diversity patterns between the PS-MPs–treated and untreated groups, with the most significant divergence observed in the high-dose (PCOS+HMP) group (Fig. 3B).

At the phylum level, PS-MPs exposure markedly increased the relative abundance of *Bacteroidetes* and

decreased *Firmicutes* compared with both the control and PCOS groups (Fig. 3C). LEfSe analysis (LDA > 3) further revealed a significant enrichment of *Bacteroides* species, particularly *Bacteroides bacterium CF*, in the high-dose (PCOS+HMP) group, whereas *Flavonifractor plautii*, *Prevotella koreensis*, and *Prevotella buccae* were dominant in controls (Fig. 3D). As a result, the *Firmicutes*/*Bacteroidetes* ratio was substantially reduced in PS-MPs–exposed mice, indicating a microbial shift toward a pro-inflammatory intestinal environment and disrupted gut homeostasis (Fig. 3E). Further analysis showed that the relative abundance of *Flavonifractor plautii* and *Prevotella buccae* decreased in a dose-dependent manner, whereas *Bacteroides bacterium CF* increased progressively with rising PS-MPs exposure levels (Fig. 3F–H). Moreover, *Flavonifractor plautii* abundance was negatively correlated with serum testosterone levels, suggesting a potential protective role against hyperandrogenism (Fig. 3I).

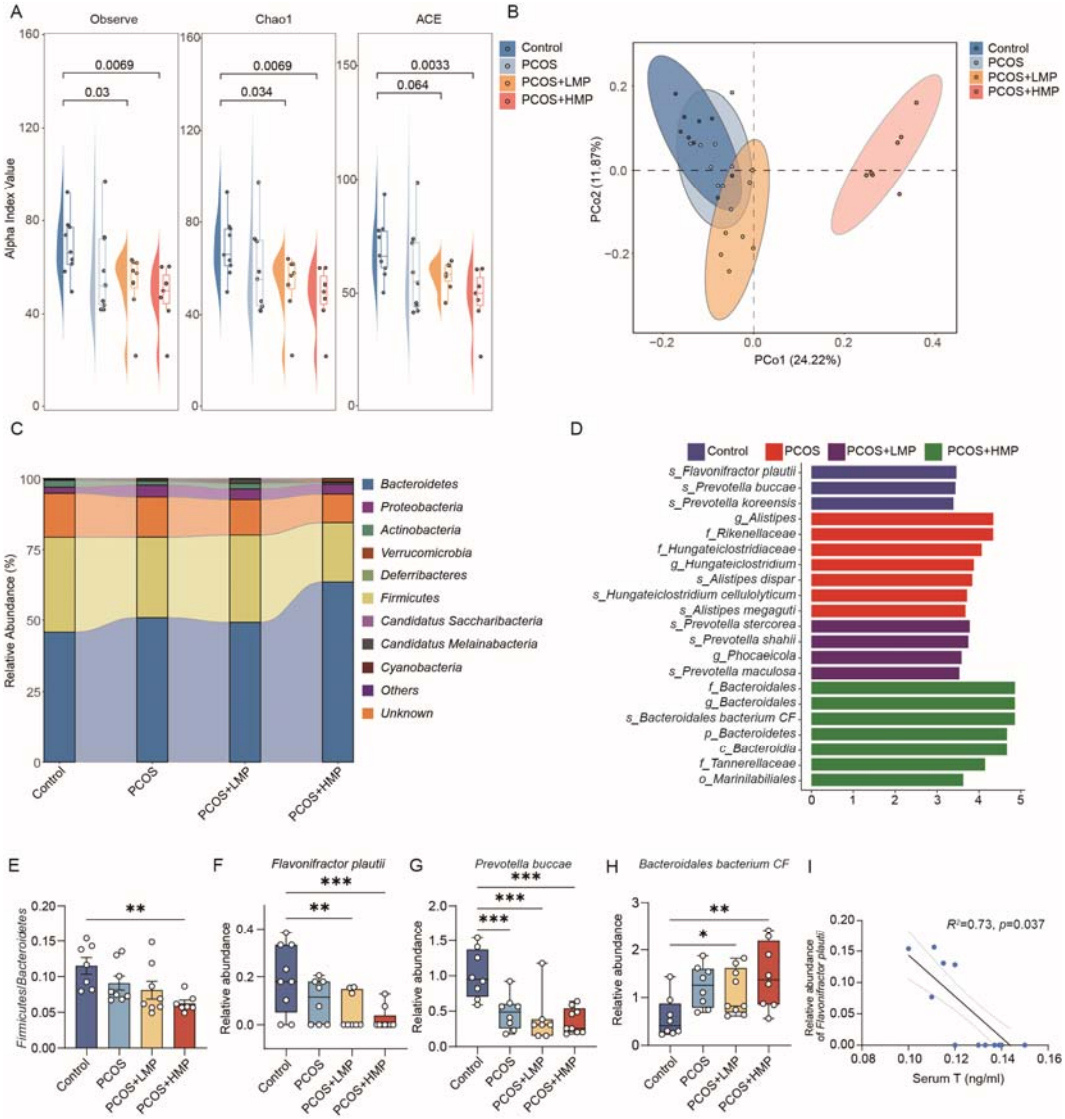

Fig. 3 PS-MPs exposure disrupts gut microbial composition in PCOS mice.
(A) Alpha diversity indices (Observed species, Chao1, and ACE) of gut microbiota. (B) Principal coordinate analysis (PCoA) based on Bray–Curtis distances. (C) Relative abundance of bacterial phyla in each group. (D) LEfSe analysis showing taxa with significant differences among groups (LDA > 3). (E) Ratio of Firmicutes to Bacteroidetes. (F–H) Relative abundances of *Flavonifractor plautii*, *Prevotella buccae*, and *Bacteroides bacterium CF* determined by 16S rRNA sequencing. (I) Correlation analysis between *Flavonifractor plautii* abundance and serum testosterone concentration. Data are presented as mean±standard deviation (SD). Results were analyzed by unpaired t test (A) and one-way ANOVA followed by Tukey's post hoc test (E, F, G and H). $^{*}P < 0.05$, $^{**}P < 0.01$, $^{***}P < 0.001$.

3.5 PS-MPs exposure reduces the synthesis of vitamin B6 via gut microbiota

The gut is crucial for nutrient metabolism, with commensal microorganisms playing a key role in regulating host metabolic processes[13,42]. To investigate how PS-MPs influence gut-derived metabolites, we conducted LC–MS/MS-based metabolomic profiling of fecal samples from both PS-MPs–treated and untreated PCOS mice. OPLS-DA analysis revealed distinct metabolic separation, accounting for 13.1% of the variance when compared to the DHEA group (Fig. 4A). Volcano plot analysis identified 81 metabolites that were upregulated and 137 that were downregulated in the high-dose (PCOS+HMP) group compared to the PCOS mice (Fig. 4B). KEGG pathway enrichment analysis highlighted that these differential metabolites were primarily involved in amino acid, bile acid, and steroid hormone metabolism, with vitamin B6 metabolism emerging as one of the most significantly enriched pathways (Fig. 4C).

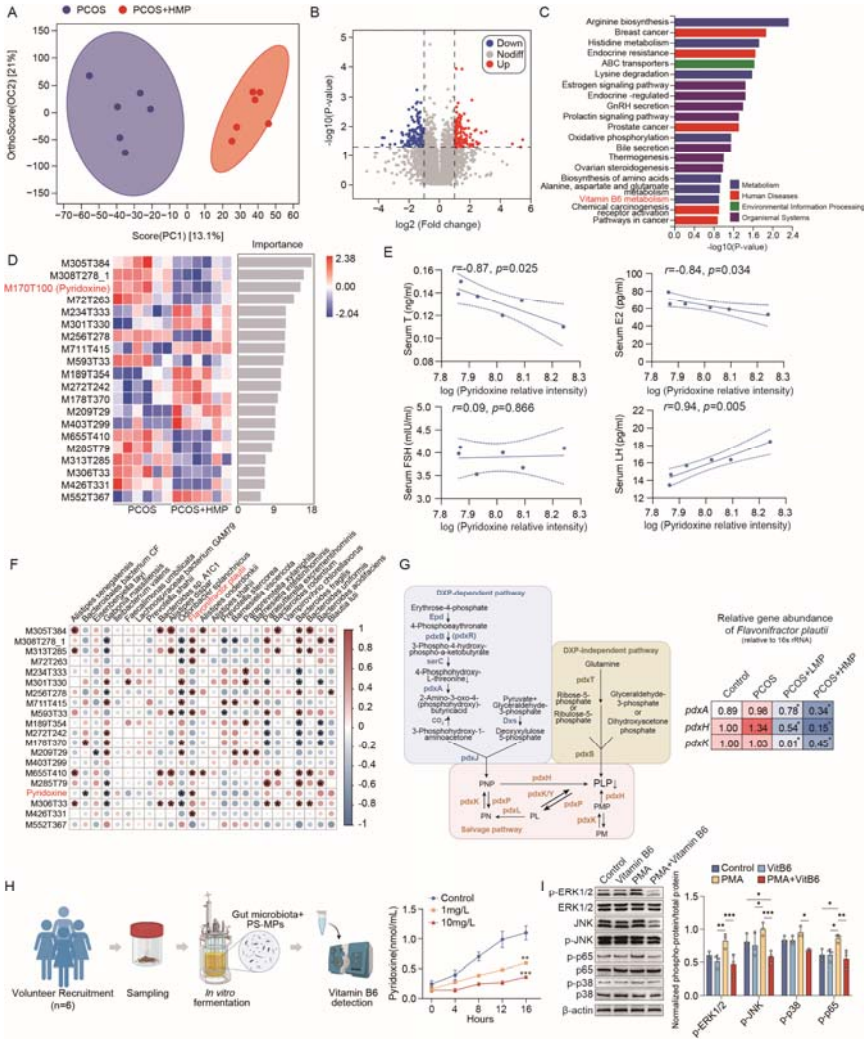

Fig. 4 PS-MPs exposure reduces the synthesis of vitamin B6 via gut microbiota.
(A) OPLS-DA score plot of fecal metabolites from PCOS and PCOS+HMP mice. (B) Volcano plot showing differential metabolites between groups. (C) KEGG pathway enrichment analysis of significantly altered metabolites. (D) Heatmap of differential metabolites identified by VIP scores, with pyridoxine (vitamin B6) highlighted. (E) Correlation analysis between fecal pyridoxine levels and serum hormone concentrations. (F) Correlation matrix between key gut microbial species and differential metabolites related to vitamin B6 metabolism. (G) Schematic representation of vitamin B6 biosynthesis and salvage pathways, and relative mRNA expression of vitamin B6–related genes in *Flavonifractor plautii*. (H) *In vitro* fermentation experiments for vitamin B6 determination after PS-MPs treat. (I) Western blot analysis of ERK1/2, JNK, p38, and NF-κB p65 phosphorylation in granulosa cells treated with PMA in the presence or absence of vitamin B6. Data are presented as mean±standard deviation (SD). Results were analyzed by one-way ANOVA followed by Dunnett's T3 multiple comparisons test (H and I). $^{*}P < 0.05$, $^{**}P < 0.01$, $^{***}P < 0.001$.

Machine learning analysis highlighted pyridoxine (vitamin B6) as a key metabolite influenced by PS-MPs exposure. As a crucial anti-inflammatory cofactor involved in microbial balance, pyridoxine levels in feces were significantly decreased following PS-MPs treatment (Fig. 4D; $P < 0.001$ for PCOS+HMP vs. PCOS). Moreover, pyridoxine concentrations showed a negative correlation with serum testosterone (T) and estrogen (E2), while being positively correlated with luteinizing hormone (LH), suggesting a link between vitamin B6 deficiency and endocrine disruption (Fig. 4E).

Microbial–metabolite correlation mapping identified 97 significant associations, with vitamin B6 levels negatively correlated with *Bacteroides bacterium CF*, *Gabonia massiliensis*, and *Odoribacter splanchnicus*, and positively correlated with *Flavonifractor plautii* (Fig. 4F). Notably, *Flavonifractor plautii*, a key vitamin B6–associated species, was significantly reduced in PS-MPs–treated mice. Consistently, gene expression analysis revealed that vitamin B6 biosynthesis–related genes regulated by *Flavonifractor plautii* were downregulated in the PCOS+HMP group compared with both control and PCOS mice (Fig. 4G).

In vitro anaerobic fermentation using fecal samples from six healthy female donors demonstrated that PS-MPs supplementation caused a dose-dependent decrease in microbial vitamin B6 synthesis capacity (Fig. 4H). Functionally, vitamin B6 supplementation inhibited PMA-induced phosphorylation of ERK1/2, JNK, p38, and NF-κB p65 in granulosa cells, thereby suppressing activation of the MAPK and NF-κB pathways (Fig. 4I).

Collectively, these results demonstrate that high-dose PS-MPs exposure disrupts gut microbiota composition and impairs microbial vitamin B6 synthesis, leading to vitamin B6 deficiency–mediated ovarian inflammation.

3.6 Gut microbiota mediates PS-MPs–induced PCOS phenotypes and impairs vitamin B6 metabolism

To determine the causal role of gut microbiota in PS-MPs–induced PCOS pathology, fecal microbiota transplantation (FMT) was performed using microbiota from control, PCOS, and PS-MPs–exposed (PCOS+HMP) donor mice (Fig. 5A). PCoA based on Bray-Curtis distances showed close clustering between donor and corresponding recipient groups, confirming successful microbial transplantation (Fig. 5B).

Compared with control-FMT and PCOS-FMT recipients, HMP-FMT mice exhibited significantly higher body weight (Fig. 5C), impaired glucose tolerance (Fig. 5D), and reduced insulin sensitivity (Fig. 5E), indicating that PS-MPs–altered microbiota can transfer metabolic dysfunction. Hormonal profiling revealed elevated T, E2, and LH levels with reduced FSH, consistent with aggravated endocrine abnormalities (Fig. 5F). PCOS-FMT mice showed only reduced insulin sensitivity. Histological analysis revealed numerous cystic follicles and reduced corpora lutea in PCOS-FMT and HMP-FMT mice, whereas control-FMT recipients displayed normal follicular morphology (Fig. 5G and Fig. S3B). Vaginal cytology confirmed irregular estrous cycles in HMP-FMT groups compared with controls (Fig. 5H).

Consistent with earlier findings, qPCR showed a pronounced reduction in *Flavonifractor plautii* in HMP-FMT mice (Fig. 5I). Correspondingly, pyridoxine concentrations in serum, ovary, and feces were significantly lower in HMP-FMT mice than in both control-FMT and PCOS-FMT groups (Fig. 5J).

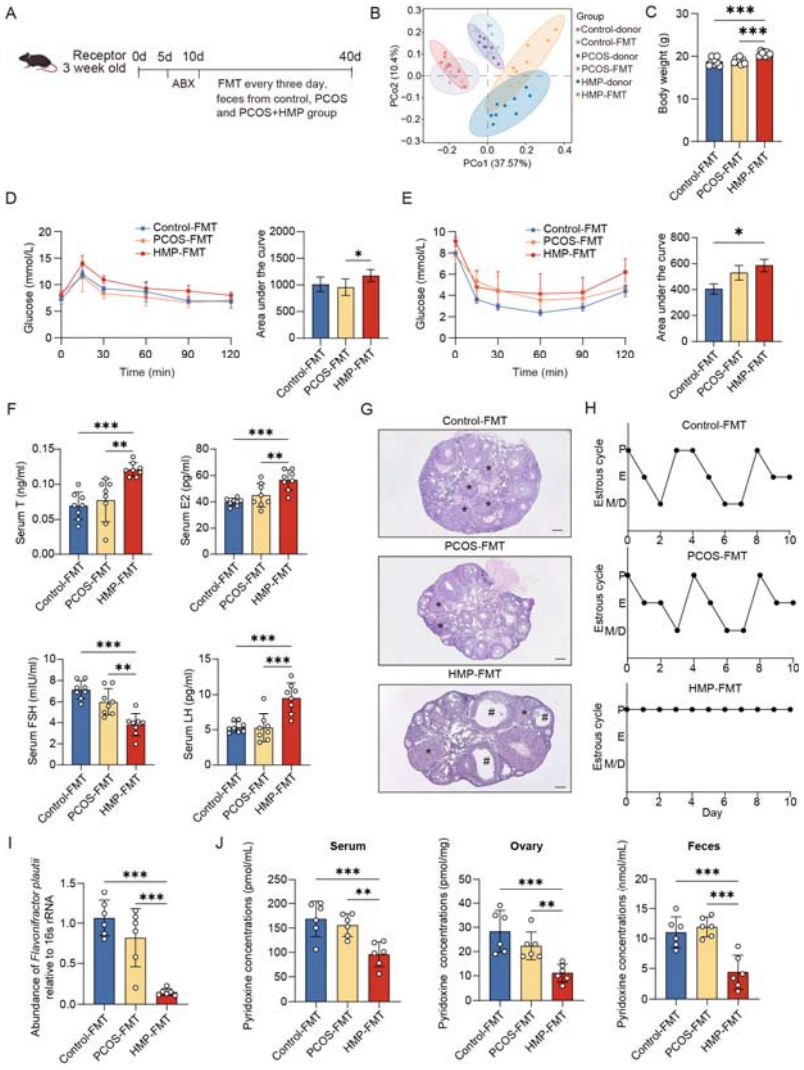

Fig. 5 Gut microbiota mediates PS-MPs–induced PCOS phenotypes.
(A) Schematic diagram of the FMT experimental design. Three-week-old recipient mice received an antibiotic cocktail (ABX) for 5 days followed by FMT every three days using feces from control, PCOS, or PCOS+HMP donor mice. (B) PCoA showing the microbial similarity between donor and recipient groups. (C) Body weight of recipient mice after FMT. (D) OGTT and corresponding area under the curve values. (E) ITT and corresponding area under the curve values. (F) Serum concentrations of T, E2, FSH, and LH determined by ELISA. (G) Representative H&E–stained ovarian sections showing follicular morphology (hash symbol, cystic follicles; asterisks, corpora lutea). Scale bar, 200 μm. (H) Estrous cycle determination based on daily vaginal cytology over 10 consecutive days. P, proestrus; E, estrus; M/D, metestrus/diestrus. (I) Quantitative PCR analysis of *Flavonifractor plautii* abundance relative to 16S rRNA. (J) Vitamin B6 (pyridoxine) concentrations in serum, ovary, and feces measured by HPLC. Data are presented as mean±standard deviation (SD). Results were analyzed by one-way ANOVA followed by Tukey's post hoc test (C, D, E, F and J) or by Dunnett's T3 multiple comparisons test (I). $*P < 0.05$, $**P < 0.01$, $***P < 0.001$.

Together, these results demonstrate that gut microbiota from PS-MPs–exposed mice can transmit both metabolic and reproductive dysfunction characteristic of PCOS, primarily through disruption of vitamin B6 metabolism.

3.7 Vitamin B6 supplementation alleviates PS-MPs–induced metabolic and ovarian dysfunction

To assess whether vitamin B6 supplementation alleviates PS-MPs–induced PCOS pathology, DHEA-treated mice exposed to PS-MPs were given vitamin B6 supplementation (PCOS+HMP+VitB6) (Fig. 6A). Vitamin B6 treatment significantly mitigated weight gain compared to PS-MPs–exposed mice (Fig. 6B; $P < 0.01$), and restored body weight to a level not statistically different from the Control group ($P > 0.05$), and

improved glucose tolerance, as evidenced by a reduced area under the OGTT curve (Fig. 6C; $P < 0.01$ vs. PCOS+HMP group; $P > 0.05$ vs. Control group). Moreover, vitamin B6 supplementation partially restored the estrous cycle disrupted by PS-MPs exposure (Fig. 6E). Hormonal profiling showed that vitamin B6 reversed the PS-MPs–induced endocrine imbalance, with FSH levels increased and LH, E2, and T levels decreased (all $P < 0.01$ vs. PCOS+HMP group), restoring them to levels close to those of the control group (Fig. 6F). Histological examination of ovaries further confirmed these improvements, with significantly fewer cystic follicles and enhanced corpora lutea formation observed in the PCOS+HMP+VitB6 group (Fig. 6G and Fig. S3C).

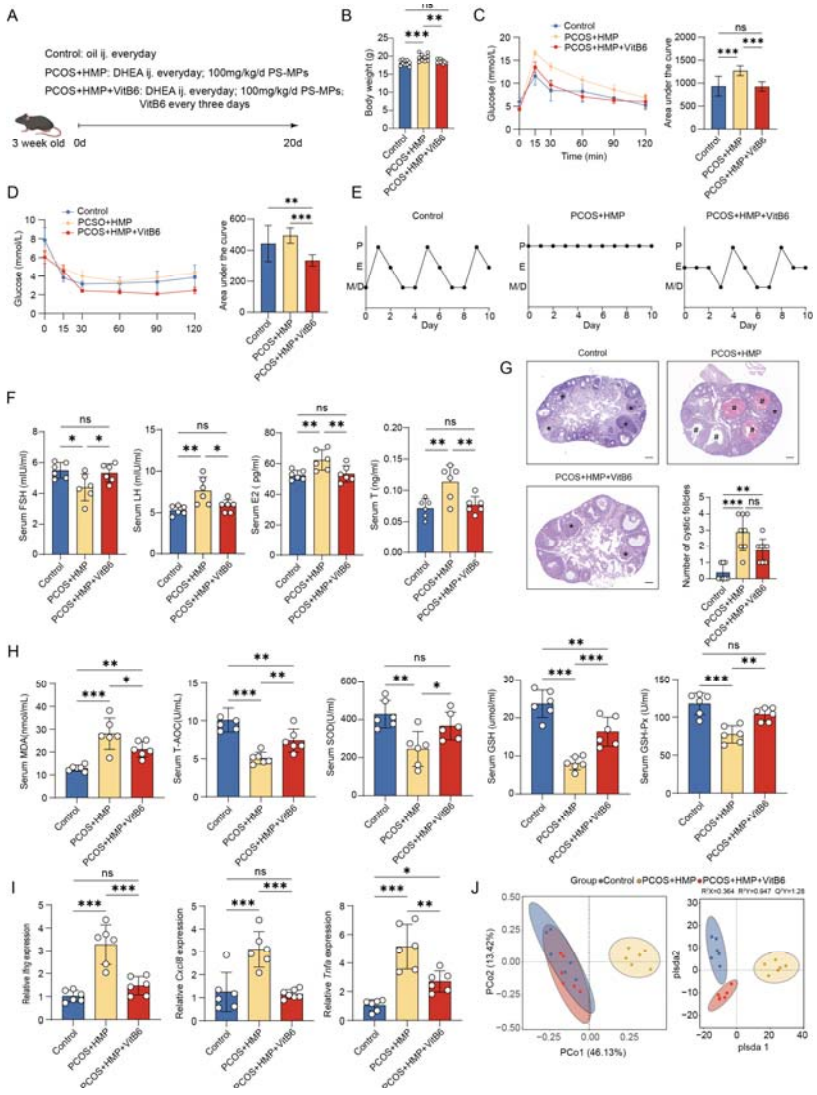

Fig. 6 Effects of vitamin B6 supplementation on PS-MPs–induced PCOS mice.
(A) Experimental design of vitamin B6 treatment in PS-MPs–exposed PCOS mice. Three-week-old mice received daily subcutaneous injections of DHEA (60 mg/kg) with or without PS-MPs (100 mg/kg/day) in drinking water for 20 days, and vitamin B6 (35 mg/mL) was administered every three days. (B) Body weight of mice in each group. (C) OGTT and area under the curve analysis. (D) ITT and area under the curve analysis. (E) Estrous cycle determination by daily vaginal smears over 10 consecutive days. P, proestrus; E, estrus; M/D, metestrus/diestrus. (F) Serum concentrations of FSH, LH, E2, and T measured by ELISA. (G) Representative H&E–stained ovarian sections showing follicular morphology (hash symbol, cystic follicles; asterisks, corpora lutea). Scale bar, 200 μm. (H) Serum oxidative stress parameters including MDA, T-AOC, SOD, GSH, and GSH-Px. (I) Relative mRNA expression levels of *Ifng*, *Cxcl8*, and *Tnfa* determined by qPCR. (J) PCoA and PLS-DA plots showing gut microbiota and metabolomic profiles among control, PCOS+HMP, and PCOS+HMP+VitB6 groups. Data are expressed as mean ± SD. Results were analyzed by one-way ANOVA followed by Tukey's post hoc test (B, C, D, F and H) or by Dunnett's T3 multiple comparisons test (G and I). ns, not significant; *$P < 0.05$, **$P < 0.01$, ***$P < 0.001$.

Oxidative stress analysis revealed that vitamin B6 supplementation notably lowered MDA levels and boosted T-AOC, SOD, GSH, and GSH-Px activities, suggesting a restoration of systemic redox balance (Fig. 6H). Inflammatory gene expression also normalized, with marked reductions in *Ifng*, *Cxcl8*, and *Tnfa* transcripts in the vitamin B6-treated group (Fig. 6I). Fecal microbiome and metabolomic profiling demonstrated that the metabolic profile of vitamin B6-treated mice was more similar to that of controls than to PS-MPs–exposed mice, indicating a significant restoration of gut microbial composition and metabolite balance (Fig. 6J).

Together, these results highlight the therapeutic potential of vitamin B6 supplementation in reversing PS-MPs–induced metabolic, oxidative, and hormonal disturbances, improving ovarian function. These findings underscore the protective role of vitamin B6 in the gut–vitamin B6–ovary axis, counteracting the reproductive toxicity induced by PS-MPs.

4. Discussion

This study delineates a novel mechanistic pathway through which microplastic exposure induces female reproductive dysfunction, specifically by exacerbating PCOS phenotypes. We demonstrate that PS-MPs exert their toxicity via a gut-mediated vitamin B6 depletion mechanism and direct provocation of ovarian oxidative stress and inflammation. Crucially, the partial reversal of these effects through oral vitamin B6 supplementation underscores the functional significance of this pathway and highlights nutritional intervention as a potential strategy to mitigate microplastic-induced reproductive damage.

These results advance the current understanding of microplastic toxicology. MPs are increasingly recognized not merely as inert particulates or passive carriers of adsorbed chemicals but as potential disruptors of host metabolism and host–microbiome co-metabolism[4,43]. The gastrointestinal tract represents the principal interface for ingested MPs and the initial site of their biological interactions. Compositional shifts in the gut microbiota following exposure likely reflect both direct particle–microbe interactions and surface-chemical perturbations that influence microbial adhesion, growth, and competitive dynamics[4]. In this study, exposure to PS-MPs was associated with significant alterations in gut microbial composition, characterized by reduced α-diversity, a decline in *Firmicutes*, and enrichment of *Bacteroidetes*—a community pattern frequently linked to inflammatory and metabolic dysregulation, particularly in PCOS[13,25]. Moreover, PS-MPs exposure selectively decreased the relative abundance of microbial taxa involved in B-vitamin biosynthetic pathways. These microbial shifts coincided with measurable reductions in intestinal and systemic vitamin B6 vitamers, suggesting that dysbiosis may impair microbially mediated vitamin B6 synthesis and thereby contribute to reduced host vitamin availability. Consistent with this interpretation, fecal microbiota transplantation from PS-MPs–exposed mice to antibiotic-treated recipients reproduced aspects of the reproductive and metabolic disturbances observed in donor animals, implying that the toxicological effects of PS-MPs are at least partly mediated through gut microbiota alterations.

Our findings further identify vitamin B6 as a potential metabolic vulnerability under PS-MPs exposure. PS-MPs exposure led to a decline in *Firmicutes*, key players in gut B vitamin metabolism[28]. This was

particularly evident in *Flavonoider plautii*, as evidenced by a significant reduction in the abundance of its vitamin B6 metabolism genes in fecal samples. This compositional shift was accompanied by declines in pyridoxal 5′-phosphate (PLP) and related vitamers in both intestinal contents and plasma. Mechanistically, PLP serves as an essential cofactor for transamination and decarboxylation reactions, supports glutathione synthesis via amino acid metabolism, and modulates cytokine production [26,27]. Therefore, a decrease in vitamin B6 is expected to weaken antioxidant defenses, increase reactive oxygen species, and amplify inflammatory signals, which is consistent with our observations. In parallel, PLP-dependent enzymes regulate one-carbon and amino acid fluxes influencing methionine–homocysteine balance[44]; disruption of these pathways may impair hormone and compromise follicular integrity[45,46]. Our observations revealed that these metabolic and redox perturbations converge at the ovary, where PS-MPs exposure was associated with increased pro-inflammatory cytokines, oxidative stress, and activation of MAPK and NF-κB signaling—molecular signatures consistent with PCOS and environmentally induced ovarian dysfunction[47,48]. Notably, vitamin B6 supplementation partially restored metabolic and reproductive parameters, supporting the view that B6 depletion represents a mechanistically relevant mediator rather than an incidental correlate of PS-MPs exposure.

The molecular mechanisms by which vitamin B6 ameliorates PCOS symptoms likely reflect its pleiotropic role as an essential enzymatic cofactor. Its active form, pyridoxal 5′-phosphate (PLP), serves as a coenzyme for over 150 reactions relevant to PCOS pathophysiology. First, PLP is required for glutathione (GSH) synthesis via the transsulfuration pathway, and restoration of GSH and antioxidant enzyme activities (SOD, GSH-Px) following B6 supplementation (Fig. 6H) counteracts PS-MP–induced oxidative stress in ovarian granulosa cells and oocytes. Second, PLP modulates inflammatory signaling, in part by suppressing NF-κB and MAPK activation. Consistent with this, our in vitro data show that vitamin B6 inhibited PMA-induced phosphorylation of NF-κB p65 and MAPK family members (ERK, JNK, and p38) in granulosa cells (Fig. 4I). Third, PLP-dependent enzymes participate in steroid hormone synthesis and degradation; thus, vitamin B6 deficiency may promote androgen excess. Accordingly, vitamin B6 supplementation normalized serum testosterone and estrogen levels (Fig. 6F). Collectively, these findings suggest that microplastics can act as ecological stressors, reconfiguring intestinal microbial networks and altering their metabolic outputs, with downstream consequences for host redox balance and reproductive health.

An important question raised by our findings is whether depletion of other microbiota-derived B vitamins similarly contributes to PCOS progression. The gut microbiome is a major source of B vitamins, including riboflavin (B2), folate (B9), and cobalamin (B12), which are central to one-carbon metabolism and thus essential for DNA synthesis, methylation, and redox homeostasis. Notably, folate and B12 regulate homocysteine metabolism, and disturbances in one-carbon metabolism with elevated homocysteine levels have been reported in PCOS patients. It is therefore plausible that PS-MP–induced dysbiosis concurrently reduces the microbial synthesis or bioavailability of multiple B vitamins, leading to a compounded micronutrient deficiency that exacerbates metabolic and reproductive dysfunction. Future studies profiling a

broader range of B vitamins and related metabolites under microplastic exposure are needed to determine whether the proposed "gut–vitamin–ovary" axis is specific to vitamin B6 or reflects a more general mechanism of microplastic-induced endocrine disruption.

PS-MPs thus emerge as modulators of host–microbe co-metabolism, linking environmental exposure to systemic metabolic and endocrine dysfunction. Beyond the context of PCOS, chronic exposure to microplastics and other environmental particulates may progressively erode micronutrient homeostasis and destabilize host–microbiome symbiosis. If PS-MPs impair microbial vitamin synthesis, other pollutants may disrupt distinct metabolic circuits, collectively reshaping host susceptibility to chronic disease. The partial restoration achieved through vitamin B6 supplementation underscores both the adaptability of the gut–vitamin–ovary axis and the potential of targeted micronutrient support to mitigate pollution-induced metabolic stress.

While vitamin B6 depletion emerges as a central mediator of the observed phenotype, the incomplete rescue by supplementation indicates that additional pathways contribute to PS-MPs–induced toxicity. Beyond its effects on microbial vitamin synthesis, PS-MPs exposure may act directly on the gut epithelium, promoting oxidative stress, increasing epithelial permeability, and facilitating translocation of microbial products such as lipopolysaccharide that amplify systemic inflammation[49,50]. Furthermore, the surface chemistry of microplastics and the presence of sorbed co-pollutants may deliver bioactive molecules capable of modulating host signaling independently of microbiome alterations[4]. Moreover, although direct ovarian invasion by PS-MPs was not demonstrated in this study, the detection of microplastics in follicular fluid in previous reports raises the possibility that particle translocation could represent an additional pathway contributing to reproductive toxicity[51], a hypothesis that warrants direct examination in future work. Our results from the PS-MPs-alone group directly address this question. While high-dose PS-MPs alone caused mild metabolic changes, they did not elicit hallmark PCOS features such as hyperandrogenism, cystic ovaries, or luteal deficiency (Fig. 1F, G, S4). Thus, within our experimental frame, PS-MPs are not a standalone inducer of PCOS. Rather, they primarily exacerbate an underlying endocrine-metabolic dysfunction, as seen in the markedly worse phenotypes of PCOS+PS-MPs mice versus either condition alone. This points to a model of environmental co-factor potentiation, in which microplastics act as metabolic and inflammatory stressors that amplify pathology in a susceptible host.

The selection of the low (2 mg/kg/day) and high (100 mg/kg/day) dose bounds, rather than a dose near the estimated human median, was intentional and aligned with the primary mechanistic goals of this study. While a median environmentally relevant dose is crucial for direct risk assessment, our aim was to establish a clear dose-response relationship and to amplify phenotypic readouts within a defined experimental window to facilitate mechanistic discovery. The high dose served to ensure robust biological signals for downstream omics and pathway analyses. Importantly, even the low dose, which falls within the lower range of human-equivalent exposure, induced significant exacerbation of PCOS traits compared to the PCOS-only group, suggesting that effects may occur at exposure levels relevant to human populations. Future chronic exposure

studies employing a gradient of environmentally realistic concentrations will be essential to refine the dose-response curve and for quantitative risk translation.

This study has several limitations. First, the DHEA-induced mouse model captures key PCOS features but does not reflect the full heterogeneity of human PCOS, warranting validation in additional models. Second, we used pristine, monodisperse PS-MPs, whereas environmental microplastics are heterogeneous and may exhibit different bioavailability and toxicity. Third, although FMT supports a microbiota-mediated mechanism, definitive causality within the "gut-vitamin B6-ovary" axis will require gnotobiotic or vitamin B6–deficient bacterial models. Fourth, our metabolomic analyses focused on vitamin B6, and broader microbial metabolic profiling is needed. Fifth, vitamin B6 was administered at a pharmacologic dose to test mechanistic principles, and its translational relevance and safety remain to be determined. Finally, ovarian transcriptomics was performed on whole tissue, limiting cell-type resolution, although granulosa cell experiments confirmed the functional relevance of key pathways.

In summary, microplastic ingestion disrupts gut microbial homeostasis and vitamin B6 metabolism, triggering systemic oxidative and inflammatory stress that impairs ovarian function. Supplementation with vitamin B6 partially reversed these effects by rebalancing gut microbiota and restoring endocrine stability. Collectively, these results highlight the gut–vitamin–ovary axis as a central mediator of environmental reproductive toxicity and underscore micronutrient maintenance as a promising avenue to mitigate the adverse health impacts of microplastic exposure.

CRediT authorship contribution statement

Yue Pan, Xiaoqin Zeng, Shulei Chen: Conceptualization, Methodology, Investigation, Writing – original draft, Writing – review & editing; Ziwei Zhou: Data curation, Investigation; Yanzhen Ye: Data curation, Formal analysis; Zhihua Zuo: Data curation, Formal analysis; Shanshui Zeng: Data curation; Xiaodong Fu: Project administration, Writing – review & editing; Yan Long: Project administration, Writing – review & editing; Zuman Dou: Project administration, Writing – review & editing; Min Jiang: Conceptualization, Project administration, Supervision, Funding acquisition.

Declaration of Competing Interest

The authors declare that they have no competing interests.

Data Availability

The data that support the findings of this study are openly available in China National Center for Bioinformation (CNCB) at https://ngdc.cncb.ac.cn/bioproject/browse/PRJCA050600, reference number PRJCA050600. This paper does not include the original code.

Acknowledgements

This work was supported by the National Natural Science Foundation of China (Grant No. 82301906), the Natural Science Foundation of Guangxi Zhuang Autonomous Region (Grant No. 2025GXNSFBA069019),

China Postdoctoral Science Foundation (2025M782044), Maternal and Child Nutrition and Health Research Project of the Maternal and Child Health Center of the National Health Commission (2024FYH21), the Natural Science Foundation of Xiamen, China (Grant No. 3502Z202571052), the Natural Science Fund of Guangdong Province (Grant No. 2022A1515012280), the Science and Technology Program of Guangzhou (Grant No. 2025A04J3729), and the Foundation for Cultivated Young Talents of Fujian Province, China (Grant No. 2025350350).

Reference

1. Zhang, K., Hamidian, A.H., Tubić, A., Zhang, Y., Fang, J.K.H., Wu, C., and Lam, P.K.S. (2021). Understanding plastic degradation and microplastic formation in the environment: A review. Environmental Pollution *274*, 116554. https://doi.org/10.1016/j.envpol.2021.116554.
2. Jadhav, E.B., Sankhla, M.S., Bhat, R.A., and Bhagat, D.S. (2021). Microplastics from food packaging: An overview of human consumption, health threats, and alternative solutions. Environmental Nanotechnology, Monitoring & Management *16*, 100608. https://doi.org/10.1016/j.enmm.2021.100608.
3. Mamun, A.A., Prasetya, T.A.E., Dewi, I.R., and Ahmad, M. (2023). Microplastics in human food chains: Food becoming a threat to health safety. Science of The Total Environment *858*, 159834. https://doi.org/10.1016/j.scitotenv.2022.159834.
4. Vethaak, A.D., and Legler, J. (2021). Microplastics and human health. Science *371*, 672–674. https://doi.org/10.1126/science.abe5041.
5. Kadac-Czapska, K., Ośko, J., Knez, E., and Grembecka, M. (2024). Microplastics and Oxidative Stress—Current Problems and Prospects. Antioxidants *13*, 579. https://doi.org/10.3390/antiox13050579.
6. Pulvirenti, E., Ferrante, M., Barbera, N., Favara, C., Aquilia, E., Palella, M., Cristaldi, A., Conti, G.O., and Fiore, M. (2022). Effects of Nano and Microplastics on the Inflammatory Process: In Vitro and In Vivo Studies Systematic Review. FBL *27*, 287. https://doi.org/10.31083/j.fbl2710287.
7. Thin, Z.S., Raja Ali, R.A., and Gew, L.T. (2025). Ecotoxicity of microplastics and nanoplastics in endocrine systems: a systematic review. Toxicol. Environ. Health Sci. https://doi.org/10.1007/s13530-025-00269-5.
8. Hassan, S., Thacharodi, A., Priya, A., Meenatchi, R., Hegde, T.A., R, T., Nguyen, H.T., and Pugazhendhi, A. (2024). Endocrine disruptors: Unravelling the link between chemical exposure and Women's reproductive health. Environ Res *241*, 117385. https://doi.org/10.1016/j.envres.2023.117385.
9. Rutkowska, A., and Rachoń, D. (2014). Bisphenol A (BPA) and its potential role in the pathogenesis of the polycystic ovary syndrome (PCOS). Gynecological Endocrinology.
10. Vagi, S.J., Azziz-Baumgartner, E., Sjödin, A., Calafat, A.M., Dumesic, D., Gonzalez, L., Kato, K., Silva, M.J., Ye, X., and Azziz, R. (2014). Exploring the potential association between brominated diphenyl ethers, polychlorinated biphenyls, organochlorine pesticides, perfluorinated compounds, phthalates, and bisphenol a in polycystic ovary syndrome: a case–control study. BMC Endocr Disord *14*, 86. https://doi.org/10.1186/1472-6823-14-86.
11. International evidence-based guideline for the assessment and management of polycystic ovary syndrome – 2023 (2023). RE, 59–79. https://doi.org/10.18370/2309-4117.2023.69.59-79.
12. Stener-Victorin, E., Teede, H., Norman, R.J., Legro, R., Goodarzi, M.O., Dokras, A., Laven, J., Hoeger, K., and Piltonen, T.T. (2024). Polycystic ovary syndrome. Nat Rev Dis Primers *10*, 27. https://doi.org/10.1038/s41572-024-00511-3.
13. Qi, X., Yun, C., Sun, L., Xia, J., Wu, Q., Wang, Y., Wang, L., Zhang, Y., Liang, X., Wang, L., et al. (2019). Gut microbiota-bile acid-interleukin-22 axis orchestrates polycystic ovary syndrome. Nat Med *25*, 1225–1233. https://doi.org/10.1038/s41591-019-0509-0.
14. Rutkowska, A.Z., and Diamanti-Kandarakis, E. (2016). Polycystic ovary syndrome and environmental toxins. Fertil Steril *106*, 948–958. https://doi.org/10.1016/j.fertnstert.2016.08.031.
15. Zhao, T., Shen, L., Ye, X., Bai, G., Liao, C., Chen, Z., Peng, T., Li, X., Kang, X., and An, G. (2023). Prenatal and postnatal exposure to polystyrene microplastics induces testis developmental disorder and affects male fertility in mice. Journal of

Hazardous Materials *445*, 130544. https://doi.org/10.1016/j.jhazmat.2022.130544.

16. Saeed, A., Akhtar, M.F., Saleem, A., Akhtar, B., and Sharif, A. (2023). Reproductive and metabolic toxic effects of polystyrene microplastics in adult female Wistar rats: a mechanistic study. Environ Sci Pollut Res *30*, 63185–63199. https://doi.org/10.1007/s11356-023-26565-6.
17. Zhang, Y., Wang, S., Olga, V., Xue, Y., Lv, S., Diao, X., Zhang, Y., Han, Q., and Zhou, H. (2022). The potential effects of microplastic pollution on human digestive tract cells. Chemosphere *291*, 132714. https://doi.org/10.1016/j.chemosphere.2021.132714.
18. Turroni, S., Wright, S., Rampelli, S., Brigidi, P., Zinzani, P.L., and Candela, M. (2021). Microplastics shape the ecology of the human gastrointestinal intestinal tract. Current Opinion in Toxicology *28*, 32–37. https://doi.org/10.1016/j.cotox.2021.09.006.
19. Zmora, N., Suez, J., and Elinav, E. (2019). You are what you eat: diet, health and the gut microbiota. Nat Rev Gastroenterol Hepatol *16*, 35–56. https://doi.org/10.1038/s41575-018-0061-2.
20. Li, B., Shi, Y., Qiu, W., Lin, Q., Zeng, S., Hou, Y., Zhou, H., Chen, M., and Zhang, D. (2023). Limosilactobacillus reuteri ameliorates preeclampsia in mice via improving gut dysbiosis and endothelial dysfunction. Biomed Pharmacother *161*, 114429. https://doi.org/10.1016/j.biopha.2023.114429.
21. Van Hul, M., and Cani, P.D. (2023). The gut microbiota in obesity and weight management: microbes as friends or foe? Nat Rev Endocrinol *19*, 258–271. https://doi.org/10.1038/s41574-022-00794-0.
22. Zuo, Z., Zeng, S., Ou, X., Du, L., and Guo, Y. (2025). Gut microbiota changes in patients with hypertensive disorders and gestational diabetes in early pregnancy: a prospective cohort study. BMC Pregnancy Childbirth *25*, 791. https://doi.org/10.1186/s12884-025-07903-7.
23. Zhang, K., Yang, J., Chen, L., He, J., Qu, D., Zhang, Z., Liu, Y., Li, X., Liu, J., Li, J., et al. (2023). Gut Microbiota Participates in Polystyrene Microplastics-Induced Hepatic Injuries by Modulating the Gut–Liver Axis. ACS Nano *17*, 15125–15145. https://doi.org/10.1021/acsnano.3c04449.
24. Peng, Y., Wang, Y., Lu, J., Xie, M., Liu, J., Dong, W., and Jiang, M. (2025). Gut microbiota-mediated poly(ε-caprolactone) microplastic degradation exacerbates metabolic dysregulation. Journal of Hazardous Materials *496*, 139262. https://doi.org/10.1016/j.jhazmat.2025.139262.
25. Li, P., Xie, L., Zheng, H., Feng, Y., Mai, F., Tang, W., Wang, J., Lan, Z., Lv, S., Jayawardana, T., et al. (2025). Gut microbial-derived 3,4-dihydroxyphenylacetic acid ameliorates reproductive phenotype of polycystic ovary syndrome. Imeta *4*, e70065. https://doi.org/10.1002/imt2.70065.
26. Ueland, P.M., McCann, A., Midttun, Ø., and Ulvik, A. (2017). Inflammation, vitamin B6 and related pathways. Molecular Aspects of Medicine *53*, 10–27. https://doi.org/10.1016/j.mam.2016.08.001.
27. Stach, K., Stach, W., and Augoff, K. (2021). Vitamin B6 in Health and Disease. Nutrients *13*, 3229. https://doi.org/10.3390/nu13093229.
28. Das, P., Babaei, P., and Nielsen, J. (2019). Metagenomic analysis of microbe-mediated vitamin metabolism in the human gut microbiome. BMC Genomics *20*, 208. https://doi.org/10.1186/s12864-019-5591-7.
29. Senathirajah, K., Attwood, S., Bhagwat, G., Carbery, M., Wilson, S., and Palanisami, T. (2021). Estimation of the mass of microplastics ingested – A pivotal first step towards human health risk assessment. Journal of Hazardous Materials *404*, 124004. https://doi.org/10.1016/j.jhazmat.2020.124004.
30. Zuccarello, P., Ferrante, M., Cristaldi, A., Copat, C., Grasso, A., Sangregorio, D., Fiore, M., and Oliveri Conti, G. (2019). Exposure to microplastics (<10 μm) associated to plastic bottles mineral water consumption: The first quantitative study. Water Research *157*, 365–371. https://doi.org/10.1016/j.watres.2019.03.091.
31. Reagan-Shaw, S., Nihal, M., and Ahmad, N. Dose translation from animal to human studies revisited. https://doi.org/10.1096/fj.07-9574LSF.
32. Bárcena, C., Valdés-Mas, R., Mayoral, P., Garabaya, C., Durand, S., Rodríguez, F., Fernández-García, M.T., Salazar, N., Nogacka, A.M., Garatachea, N., et al. (2019). Healthspan and lifespan extension by fecal microbiota transplantation into progeroid mice. Nat Med *25*, 1234–1242. https://doi.org/10.1038/s41591-019-0504-5.
33. Liu, Z., Li, P., Zhao, Z.-H., Zhang, Y., Ma, Z.-M., and Wang, S.-X. (2016). Vitamin B6 Prevents Endothelial Dysfunction, Insulin Resistance, and Hepatic Lipid Accumulation in Apoe−/− Mice Fed with High-Fat Diet. Journal of Diabetes Research

2016, 1748065. https://doi.org/10.1155/2016/1748065.

34. Zeng, S., Pan, Y., Liu, F., Yin, J., Jiang, M., Long, Y., Zhao, X., Lash, G.E., and Yang, H. (2021). Role of clusterin in the regulation of trophoblast development and preeclampsia. Biochemical and Biophysical Research Communications *583*, 128–134. https://doi.org/10.1016/j.bbrc.2021.10.064.
35. Callahan, B.J., Wong, J., Heiner, C., Oh, S., Theriot, C.M., Gulati, A.S., McGill, S.K., and Dougherty, M.K. (2019). High-throughput amplicon sequencing of the full-length 16S rRNA gene with single-nucleotide resolution. Nucleic Acids Research *47*, e103. https://doi.org/10.1093/nar/gkz569.
36. Pérez-Burillo, S., Molino, S., Navajas-Porras, B., Valverde-Moya, Á.J., Hinojosa-Nogueira, D., López-Maldonado, A., Pastoriza, S., and Rufián-Henares, J.Á. (2021). An in vitro batch fermentation protocol for studying the contribution of food to gut microbiota composition and functionality. Nat Protoc *16*, 3186–3209. https://doi.org/10.1038/s41596-021-00537-x.
37. Long, Y., Zeng, S., Gao, F., Liu, F., Zhang, Y., Zhou, C., Zhu, C., Zhao, X., Han, M., Gan, Q., et al. (2022). SERPINA5 may promote the development of preeclampsia by disruption of the uPA/uPAR pathway. Transl Res, S1931-5244(22)00145-1. https://doi.org/10.1016/j.trsl.2022.06.011.
38. Dou, Z., Yu-Long, Z., Chun-Yang, T., Chuang, L., Jia-Qin, F., Qiang, H., Chun, C., Li-Jun, Y., Chin-Ping, T., Hui, N., et al. (2024). Construction of blackberry polysaccharide nano-selenium particles: Structure features and regulation effects of glucose/lipid metabolism in HepG2 cells. Food Res Int *187*, 114428. https://doi.org/10.1016/j.foodres.2024.114428.
39. Dou, Z., Tian, Y., Zhang, Y., Zhang, W., Duan, Q., Huang, Q., Zhang, B., Niu, H., Wang, L., and Zeng, S. (2025). Pectin-type polysaccharides from raspberry (Rubus idaeus L.): structure characterization and activity against DSS-induced colitis. Carbohydr Polym *364*, 123710. https://doi.org/10.1016/j.carbpol.2025.123710.
40. Lievens, S., Slegers, T., Mees, M.A., Thielemans, W., Poma, G., Covaci, A., and Van Der Borght, M. (2022). A simple, rapid and accurate method for the sample preparation and quantification of meso- and microplastics in food and food waste streams. Environmental Pollution *307*, 119511. https://doi.org/10.1016/j.envpol.2022.119511.
41. Xie, L., Chen, T., Liu, J., Hou, Y., Tan, Q., Zhang, X., Li, Z., Farooq, T.H., Yan, W., and Li, Y. (2022). Intestinal flora variation reflects the short-term damage of microplastic to the intestinal tract in mice. Ecotoxicology and Environmental Safety *246*, 114194. https://doi.org/10.1016/j.ecoenv.2022.114194.
42. Jin, Y., Lu, L., Tu, W., Luo, T., and Fu, Z. (2019). Impacts of polystyrene microplastic on the gut barrier, microbiota and metabolism of mice. Science of The Total Environment *649*, 308–317. https://doi.org/10.1016/j.scitotenv.2018.08.353.
43. Bora, S.S., Gogoi, R., Sharma, M.R., Anshu, Borah, M.P., Deka, P., Bora, J., Naorem, R.S., Das, J., and Teli, A.B. (2024). Microplastics and human health: unveiling the gut microbiome disruption and chronic disease risks. Front. Cell. Infect. Microbiol. *14*. https://doi.org/10.3389/fcimb.2024.1492759.
44. Dalto, D.B., and Matte, J.-J. (2017). Pyridoxine (Vitamin B6) and the Glutathione Peroxidase System; a Link between One-Carbon Metabolism and Antioxidation. Nutrients *9*, 189. https://doi.org/10.3390/nu9030189.
45. Allgood, V.E., and Cidlowski, J.A. (1992). Vitamin B6 modulates transcriptional activation by multiple members of the steroid hormone receptor superfamily. Journal of Biological Chemistry *267*, 3819–3824. https://doi.org/10.1016/S0021-9258(19)50599-3.
46. Mirani, M., Bahmanpour, S., Masjedi, F., Derakhshan, Z., Dara, M., Nasr-Esfahani, M.H., and Tabei, S.M.B. (2023). Pyridoxamine protects human granulosa cells against advanced glycation end-products-induced steroidogenesis disturbances. Mol Biol Rep *50*, 8537–8549. https://doi.org/10.1007/s11033-023-08723-8.
47. Abraham Gnanadass, S., Divakar Prabhu, Y., and Valsala Gopalakrishnan, A. (2021). Association of metabolic and inflammatory markers with polycystic ovarian syndrome (PCOS): an update. Arch Gynecol Obstet *303*, 631–643. https://doi.org/10.1007/s00404-020-05951-2.
48. Zeber-Lubecka, N., Ciebiera, M., and Hennig, E.E. (2023). Polycystic Ovary Syndrome and Oxidative Stress—From Bench to Bedside. International Journal of Molecular Sciences *24*, 14126. https://doi.org/10.3390/ijms241814126.
49. Huang, D., Zhang, Y., Long, J., Yang, X., Bao, L., Yang, Z., Wu, B., Si, R., Zhao, W., Peng, C., et al. (2022). Polystyrene microplastic exposure induces insulin resistance in mice via dysbacteriosis and pro-inflammation. Science of The Total Environment *838*, 155937. https://doi.org/10.1016/j.scitotenv.2022.155937.
50. Xie, S., Zhang, R., Li, Z., Liu, C., Chen, Y., and Yu, Q. (2023). Microplastics perturb colonic epithelial homeostasis associated

with intestinal overproliferation, exacerbating the severity of colitis. Environmental Research *217*, 114861. https://doi.org/10.1016/j.envres.2022.114861.

51. Montano, L., Raimondo, S., Piscopo, M., Ricciardi, M., Guglielmino, A., Chamayou, S., Gentile, R., Gentile, M., Rapisarda, P., Oliveri Conti, G., et al. (2025). First evidence of microplastics in human ovarian follicular fluid: An emerging threat to female fertility. Ecotoxicology and Environmental Safety *291*, 117868. https://doi.org/10.1016/j.ecoenv.2025.117868.